The Astrophysical Journal Letters, 978:L43 (9pp), 2025 January 10 https://doi.org/10.3847/2041-8213/ad9dde

Evaluating the Potential to Constrain Dark Matter Annihilation with Fermi-LAT Observations of Ultrafaint Compact Stellar Systems

Antonio Circiello[1], Alex McDaniel[1], Alex Drlica-Wagner[2,3,4], Christopher Karwin[5], Marco Ajello[1], Mattia Di Mauro[6], and Miguel Á. Sánchez-Conde[7,8]
[1] Department of Physics and Astronomy, Clemson University, Clemson, SC 29631, USA
[2] Fermi National Accelerator Laboratory, P.O. Box 500, Batavia, IL 60510, USA
[3] Kavli Institute for Cosmological Physics, University of Chicago, Chicago, IL 60637, USA
[4] Department of Astronomy and Astrophysics, University of Chicago, Chicago, IL 60637, USA
[5] NASA Postdoctoral Program Fellow, NASA Goddard Space Flight Center, Greenbelt, MD, 20771, USA
[6] Istituto Nazionale di Fisica Nucleare, Sezione di Torino, Via P. Giuria 1, 10125 Torino, Italy
[7] Instituto de Física Teórica UAM-CSIC, Universidad Autónoma de Madrid, C/ Nicolás Cabrera, 13-15, 28049 Madrid, Spain
[8] Departamento de Física Teórica, M-15, Universidad Autónoma de Madrid, E-28049 Madrid, Spain
Received 2024 March 29; revised 2024 November 20; accepted 2024 December 12; published 2025 January 10

Abstract

Recent results from numerical simulations and models of galaxy formation suggest that recently discovered ultrafaint compact stellar systems (UFCSs) in the halo of the Milky Way (MW) may be some of the smallest and faintest galaxies. If this is the case, these systems would be attractive targets for indirect searches of weakly interacting massive particle dark matter (DM) annihilation due to their relative proximity and high expected DM content. In this study, we analyze 14.3 yr of γ-ray data collected by the Fermi-Large Area Telescope coincident with 26 UFCSs. No significant excess γ-ray emission is detected, and we present γ-ray flux upper limits for these systems. Assuming that the UFCSs are DM-dominated galaxies consistent with being among the faintest and least massive MW dwarf spheroidal (dSph) satellite galaxies, we derive the projected sensitivity for a DM annihilation signal. We find that observations of UFCSs have the potential to yield some of the most powerful constraints on DM annihilation, with sensitivity comparable to observations of known dSphs and the Galactic center. This result emphasizes the importance of precise kinematic studies of UFCSs to empirically determine their DM content.

Unified Astronomy Thesaurus concepts: Dark matter (353); Gamma-ray astronomy (628)

1. Introduction

The Milky Way (MW) is surrounded by more than fifty dwarf spheroidal (dSph) satellite galaxies that reside in dark matter (DM) halos (e.g., J. D. Simon 2019 and references therein). While it was once possible to distinguish DM-dominated galaxies from DM-deficient star clusters based on size and luminosity (e.g., B. Willman et al. 2005), many recently discovered systems have sizes and luminosities that blur that boundary (see W. Cerny et al. 2023a and references therein). In particular, dozens of ultrafaint compact stellar systems (UFCSs) have been discovered at distances of several tens of kiloparsecs possessing low luminosities, $L_\star < 10^4 L_\odot$, and small physical sizes, $r_h < 30$ pc (see Table 1 for a list of references). Detailed kinematic studies of these systems are challenging due to their distances and low luminosities; however, recent theoretical arguments suggest that these systems could be the faintest and least massive DM-dominated galaxies (e.g., V. Manwadkar & A. V. Kravtsov 2022; R. Errani et al. 2023a). One example in this class of systems is the recently discovered satellite Ursa Major III/UNIONS I (UMa III; S. E. T. Smith et al. 2024). While measurements of the velocity dispersion of this system are inconclusive due to the small number of measured stars, simulations suggest that a DM halo is necessary to stabilize the system against tidal dissolution (R. Errani et al. 2023b). If this system is indeed a DM-dominated galaxy, then galaxy–halo modeling arguments suggest that its host DM halo had a peak mass of $\lesssim 10^8\ M_\odot$ (T. Sawala et al. 2015; E. O. Nadler et al. 2020; V. Manwadkar & A. V. Kravtsov 2022; Y. Revaz 2023). This work is based on the assumption that UMa III and other UFCSs (see Section 2) are DM dominated and that their subhaloes are similar in nature to the dSphs (V. Manwadkar & A. V. Kravtsov 2022). This second hypothesis is needed since the size of a subhalo can vary strongly depending on its tidal history. R. Errani et al. (2023a) show that the subhaloes hosting the UFCSs could have similar extensions to the dSphs or they could have been stripped by tides down to their stellar components. In order to evaluate the projected sensitivity to DM annihilation signals, we start by assuming all objects in our sample are similar in nature to the dSphs. We then evaluate how the sensitivity is affected if a subset of the targets contain much less DM than is implied by our initial assumption (see Section 5).

Under these hypotheses, the UFCSs would be powerful targets for searches of γ-ray emission from the annihilation of weakly interacting massive particle (WIMP; for reviews, see G. Jungman et al. 1996; L. Bergström 2000; A. A. Abdo et al. 2010) DM. UFCSs are an attractive target primarily due to their proximity, which could lead to a higher γ-ray flux from DM annihilation compared to the MW satellites studied previously. The detection of excess γ-ray emission coincident with one or more of these systems (especially the closest ones) would be exciting even if their DM contents have not yet been measured. On the other hand, a null detection of nearby DM-dominated UFCSs would increase the sensitivity of existing studies of dSphs, which already yield the most powerful and robust

Table 1
List of the UFCSs That Fall in the Selection Regions Highlighted in Figure 1

Name	GLon (deg)	GLat (deg)	Distance (kpc)	$R_{1/2}$ (pc)	M_V	$\log_{10}(J_{photo})$ ($\mathrm{GeV^2/cm^5}$)	F_{UL} ($\times 10^{-12}$ $\mathrm{erg/cm^2/s}$)	Reference
Nominal Sample								
Balbinot 1	75.18	−32.64	31.9	5.57	−1.2	19.43	14.07	E. Balbinot et al. (2013)
BLISS 1	290.83	19.65	23.7	4.14	0.0	19.64	15.68	S. Mau et al. (2019)
DELVE 1	14.19	30.29	19.0	6.08	−0.2	19.79	1.92	S. Mau et al. (2020)
DELVE 2	294.24	−47.79	71.0	21.48	−2.1	18.52	1.28	W. Cerny et al. (2023b)
DELVE 3	335.85	−27.06	56.0	6.52	−1.3	18.91	2.66	W. Cerny et al. (2023b)
DELVE 4	42.31	56.43	45.0	6.41	−0.2	19.06	4.76	W. Cerny et al. (2023b)
DELVE 5	19.38	61.36	39.0	7.71	0.4	19.06	4.68	W. Cerny et al. (2023b)
DELVE 6	290.57	−49.08	79.8	0.43	−1.2	15.61	1.76	W. Cerny et al. (2023a)
DES 4	270.87	−33.44	31.3	7.56	−1.1	19.37	3.43	G. Torrealba et al. (2019)
DES Sgr 2	163.58	−52.20	23.8	11.04	−1.1	19.62	1.36	E. Luque et al. (2017)
Kim 1	68.52	−38.42	19.8	6.91	0.3	19.71	2.71	D. Kim & H. Jerjen (2015)
Kim 3	310.86	31.79	15.1	2.29	0.7	20.11	4.69	D. Kim et al. (2016)
Koposov 1	260.97	70.76	48.3	8.71	−1.0	19.02	1.58	R. R. Muñoz et al. (2018)
Laevens 3	63.60	−21.18	61.4	11.43	−2.8	18.86	4.53	N. Longeard et al. (2019)
Munoz 1	105.44	45.58	45.0	6.41	−0.4	19.02	0.62	R. R. Muñoz et al. (2018)
SMASH 1	292.14	−27.99	57.0	9.45	−1.0	18.89	4.18	N. F. Martin et al. (2016)
UMa III	194.61	73.68	10.0	3.0	2.2	20.87	1.83	S. E. T. Smith et al. (2024)
Inclusive Sample								
DES 1	310.52	−67.83	76.0	5.42	−1.4	18.75	1.81	B. C. Conn et al. (2018)
DES 3	343.83	−46.51	76.2	6.21	−2.0	18.74	1.35	E. Luque et al. (2018)
DES Sgr 1	142.83	−75.79	26.5	2.71	0.3	19.64	3.40	E. Luque et al. (2017)
Eridanus III	274.95	−59.60	91.0	8.34	−2.0	18.57	0.57	B. C. Conn et al. (2018)
HSC 1	66.32	−41.84	46.0	5.89	−0.2	19.07	1.87	D. Homma et al. (2019)
Kim 2	347.15	−42.07	100.0	13.96	−3.3	18.47	2.74	D. Kim et al. (2015)
Koposov 2	195.11	25.55	34.7	4.44	−0.9	19.44	1.52	R. R. Muñoz et al. (2018)
Laevens 1	274.81	47.85	145.0	21.51	−4.8	18.17	1.67	B. P. M. Laevens et al. (2014)
PS1 1	10.04	−17.42	29.6	4.74	−1.9	19.59	5.25	G. Torrealba et al. (2019)

Note. The nominal sample includes the sources that fall below the surface brightness line $\mu = 25$ mag arcsec^{-2} . The inclusive sample contains all the sources in the nominal sample, with the addition of the sources in the region corresponding to 24 mag arcsec^{-2} $< \mu \leqslant 25$ mag arcsec^{-2} . The values of the J-factor listed here are computed using the photometric scaling relation in Equation (3) (A. B. Pace & L. E. Strigari 2019) for all systems except UMa III, where we adopt the value evaluated by M. Crnogorčević & T. Linden (2024). The J-factors and the upper limits for γ-ray flux at 95% confidence level in the [0.5 GeV–1 TeV] energy range for each source are reported in Figure 2. While we report the main reference for each source in the last column, refer to the Local Volume Database (A. Pace 2024) for a more complete list.

constraints on DM annihilation (A. McDaniel et al. 2024 and references therein).

In this Letter, we present the results of a search for γ-ray emission coincident with a sample of 26 UFCSs. Our sample was selected to be consistent with the galaxy size–luminosity relationship derived in V. Manwadkar & A. V. Kravtsov (2022). Our analysis of the Fermi-Large Area Telescope (LAT) γ-ray data adopts the procedure developed for the analysis of dSphs by A. McDaniel et al. (2024), which closely follows previous LAT analyses of dSphs (e.g., M. Ackermann et al. 2015; A. Albert et al. 2017). We find no significant excesses of γ-ray emission coincident with any of the UFCSs, and we present flux upper limits for each system. Under the assumption that the UFCSs are DM-dominated systems consistent with the known population of dSphs, we proceed to make projections for the ability to constrain the DM annihilation cross section from the null detection of γ-ray emission. We also derive sensitivity projections for a subset of 17 out of the 26 UFCSs from the initial sample, applying a more stringent selection in size–luminosity space. We find that, although subject to large uncertainties at present, the DM cross-section upper limits derived under these assumptions for both samples of UFCSs are more sensitive than those obtained from recent dSph analyses (e.g., M. Di Mauro et al. 2023; A. McDaniel et al. 2024), emphasizing the importance of kinematic studies of UFCSs to empirically determine their DM content.

The Letter is organized as follows. In Section 2, we discuss how our samples of UFCSs were selected. In Section 3, we detail the assumed model for the DM halos of UFCSs as well as the DM annihilation channels considered. Section 4 is devoted to the Fermi-LAT data selection and the analysis procedure. Finally, in Section 5, we discuss the results and conclude.

2. Sample Selection

The populations of DM-dominated dSphs and DM-deficient classical globular clusters have historically been separable in the space of size (as indicated by the half-light radius) and luminosity (Figure 1). However, as the sensitivity of optical imaging surveys has increased, fainter and more compact systems have been discovered populating a region of parameter space where their classification is uncertain (e.g., J. D. Simon 2019; A. Drlica-Wagner et al. 2020). Furthermore, the low luminosities and distances of these systems make it difficult to measure the velocities of enough member stars to confidently determine velocity dispersions and dynamical masses. Early observational studies assumed that these systems

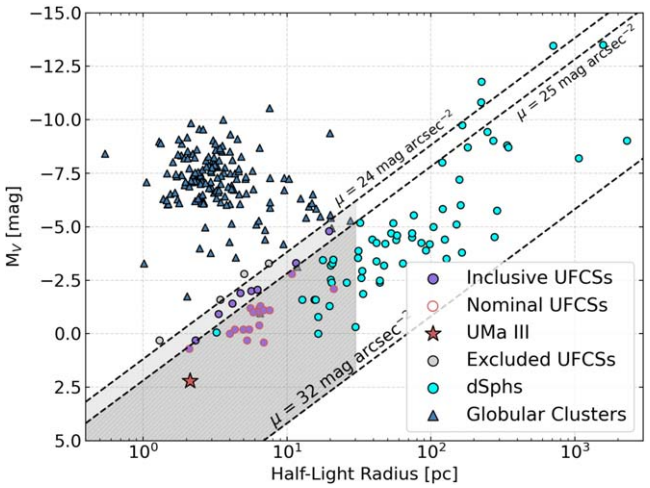

Figure 1. *V*-band absolute magnitude vs. physical half-light radius for MW globular clusters, dSphs, and UFCSs. The dashed lines mark the minimum surface brightness used to select the inclusive ($\mu > 24$ mag arcsec^{-2}) and nominal ($\mu > 25$ mag arcsec^{-2}) samples, based on the model of V. Manwadkar & A. V. Kravtsov (2022). The light and dark gray-shaded areas represent the regions of inclusive and nominal selections, respectively. The purple points are the UFCSs in the inclusive sample. The UFCSs that are also included in the nominal sample are circled in red. A complete list of both samples is reported in Table 1. The gray points are the UFCSs that fall outside our selections and were excluded from the analysis for this reason. The cyan points are the confirmed dSphs from `dmsky` (https://github.com/fermiPy/dmsky). The dark blue triangles are the confirmed globular clusters from the Local Volume Database (A. Pace 2024).

were a low-luminosity tail of the globular cluster population, possibly formed and accreted within satellite galaxies that were subsequently disrupted (e.g., S. Mau et al. 2019). However, recent theoretical modeling work has suggested that the population of dwarf galaxies may extend to equivalently small sizes (e.g., V. Manwadkar & A. V. Kravtsov 2022; R. Errani et al. 2023a). In particular, the regulator model of galaxy formation developed in A. Kravtsov & V. Manwadkar (2022) and applied to simulations of a Milky Way–like system in V. Manwadkar & A. V. Kravtsov (2022) predicts that a significant population of compact, low-luminosity satellite galaxies exists.

We select a sample of UFCSs that are consistent in physical size and absolute magnitude with the locus of galaxies produced by the model of V. Manwadkar & A. V. Kravtsov (2022, see their Figure 12). In particular, we select UFCSs that have azimuthally averaged physical half-light radii $r_{1/2} < 30$ pc and surface brightnesses of 24 mag arcsec$^{-2} < \mu_V < 32$ mag arcsec^{-2}. Furthermore, we remove systems that have previously been included in population studies of γ-ray emission from dSphs (Bootes V, Cetus II, Draco II, Grus I, Leo Minor I, Pictor I, Segue 1, Segue 3, Triangulum II, Tucana V, Virgo II, and Willman 1; e.g., A. Albert et al. 2017; A. McDaniel et al. 2024) or have been confirmed to be DM deficient from kinematic measurements (AM 4, Palomar 5, Palomar 13, and Palomar 14; W. E. Harris 1996). We apply the same selection criteria used for the dSphs in A. McDaniel et al. (2024) to avoid contamination from other sources of γ-ray emission by checking if any targets in our sample fall within the 95% confidence radius of a 4FGL-DR4 source or within $0.^{\circ}1$ (i.e., roughly the mean of the 95% confidence radius of point sources in the 4FGL; J. Ballet et al. 2023) of a source in the BZCat, CRATES, and WIBRaLS catalogs. No targets were removed by this criteria. We refer to UFCSs passing this selection as the "inclusive sample," which contains 26 targets (Table 1). We also analyze a subset of this sample, selecting targets in a more restrictive range of surface brightness (25 mag arcsec$^{-2} < \mu_V < 32$ mag arcsec^{-2}), which corresponds to the region of maximum density of galaxies predicted by V. Manwadkar & A. V. Kravtsov (2022). We refer to this selection as our "nominal sample," which contains 17 of the 26 UFCSs from the inclusive sample. Targets that fall into this selection are listed separately in Table 1.

3. DM Annihilation

Astrophysical searches for DM involve looking for the signatures of DM interactions. In the WIMP DM model, one possible signature of DM annihilation is γ-ray emission through the production of high-energy standard model particles (e.g., G. Bertone et al. 2005 for a review). The expected γ-ray flux from DM annihilation is (P. Ullio et al. 1998)

$$\frac{d\Phi_\chi}{dE} = J \times \frac{1}{4\pi}\frac{\langle\sigma v\rangle}{2M_\chi^2}\sum_i \beta_i \frac{dN_i}{dE}, \quad (1)$$

where M_χ is the rest mass of the DM particle, and $\langle\sigma v\rangle$ is the velocity-averaged DM annihilation cross section. The sum is performed over the annihilation channels, where β_i is the branching ratio for the ith channel. The γ-ray spectrum per annihilation event given the annihilation channel, dN/dE, is given by the DM model that is being considered. In this work, we use the PPPC4DMID[9] tables from M. Cirelli et al. (2011) to compute the different annihilation spectra. The annihilation channels considered are $b\bar{b}$ and $\tau^+\tau^-$.[10] These two annihilation channels are typically chosen as representative because their spectra enclose most of the shapes of the other annihilation channels (M. Cirelli et al. 2011). Electroweak corrections are taken into account only for the $\tau^+\tau^-$ channel, as they have a minimal effect in the $b\bar{b}$ channel (P. Ciafaloni et al. 2011). The "*J*-factor" (J) is a geometrical quantity obtained by integrating the squared density (ρ_χ^2) of DM along the line of sight (l.o.s., ℓ) and the solid angle ($\Delta\Omega$):

$$J = \int_{\Delta\Omega}\int_{\text{l.o.s.}} \rho_\chi^2 \, d\ell \, d\Omega. \quad (2)$$

While the DM density profile of a system can be inferred from a dynamical Jeans analysis of its member stars (e.g., V. Bonnivard et al. 2015; A. B. Pace & L. E. Strigari 2019), spectroscopic measurements are currently unavailable for many faint systems, making a direct determination of the *J*-factor impossible. Several previous γ-ray studies (e.g., A. Drlica-Wagner et al. 2015; A. Albert et al. 2017; A. McDaniel et al. 2024) have estimated the *J*-factors for targets that lacked direct measurements through scaling relations with the kinematic or photometric properties of the system (e.g., A. Drlica-Wagner et al. 2015; N. W. Evans et al. 2016; A. B. Pace & L. E. Strigari 2019). In this analysis, we use the most recent versions of these relations from

[9] http://www.marcocirelli.net/PPPC4DMID.html

[10] In a recent work by C. Arina et al. (2024) the authors have computed updated source spectra for γ-rays from DM, which, for the annihilation channels used in this Letter, are similar to the one obtained in the PPPC4DMID.

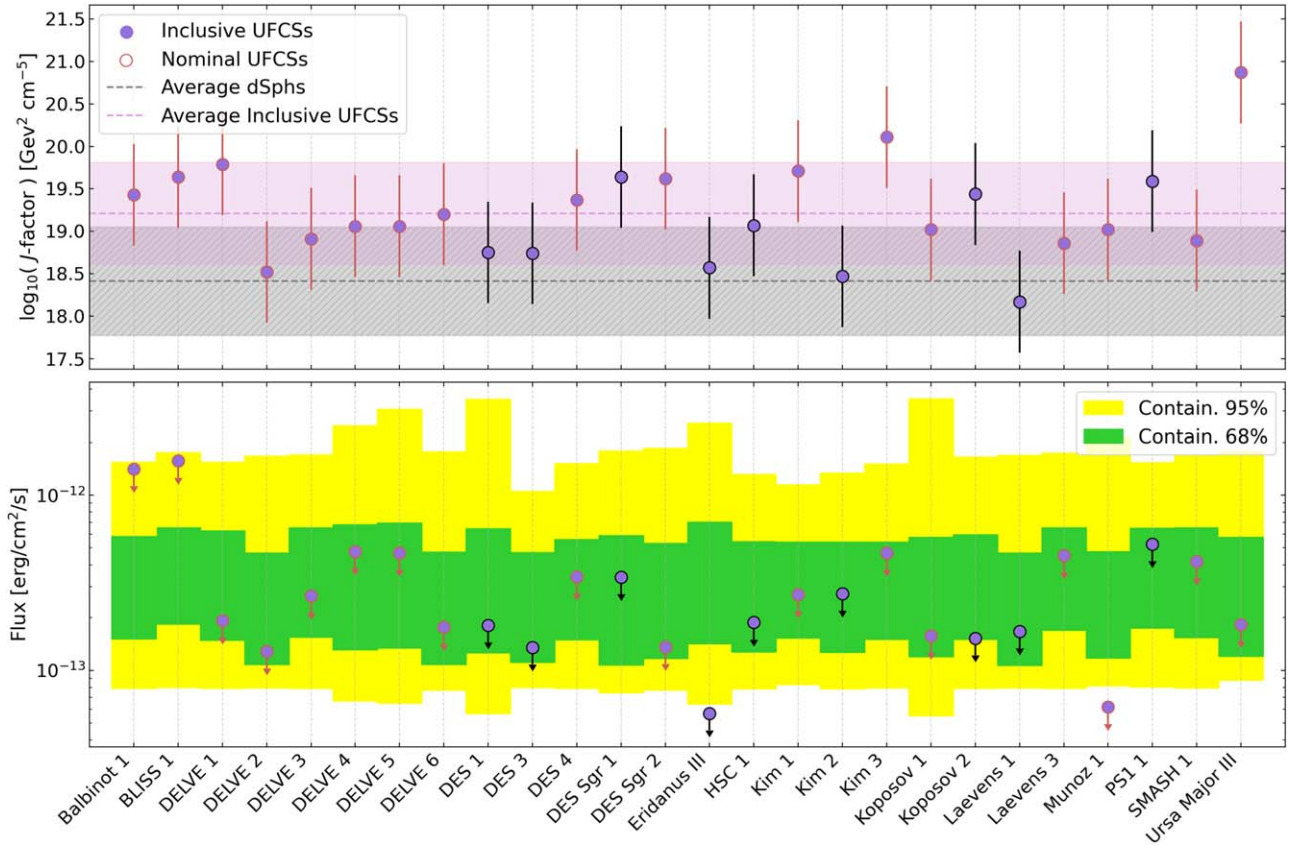

Figure 2. Top: *J*-factor for the selected UFCSs derived using the scaling relations of A. B. Pace & L. E. Strigari (2019). We use the photometric *J*-factor relation (Equation (3)) for all the sources except UMa III, which is instead derived from the velocity dispersion scaling relation of A. B. Pace & L. E. Strigari (2019) as reported by M. Crnogorčević & T. Linden (2024). We included the average *J*-factors, with their uncertainties, for the dSphs (gray band) and the inclusive sample of UFCSs (purple band) Bottom: γ-ray flux upper limits in the [0.5 GeV–1 TeV] energy band at 95% confidence level for the selected UFCSs. The green and yellow containment bands are obtained by selecting blank fields that reside at the same Galactic latitude as each target (within $\pm 5^{\circ}$).

A. B. Pace & L. E. Strigari (2019):

$$\frac{J_{\rm photo}(0.5\circ)}{\rm GeV^2\ cm^{-5}} \simeq 10^{18.17}\left(\frac{L_V}{10^4 L_\odot}\right)^{0.23}\left(\frac{d}{100\ \rm kpc}\right)^{-2}\left(\frac{r_{1/2}}{100\rm pc}\right)^{-1} \quad (3)$$

to estimate the *J*-factor from photometric properties. In this equation, d is the distance to the system, $r_{1/2}$ is the azimuthally averaged physical half-light radius, and L_V is the *V*-band luminosity. Since none of the targets in our sample have confidently measured velocity dispersions, the *J*-factors used in this analysis are computed from Equation (3) with the exception of UMa III, for which we use the value obtained by M. Crnogorčević & T. Linden (2024) from the velocity dispersion scaling relation from A. B. Pace & L. E. Strigari (2019), rather than the photometric one in Equation (3).

In previous dSph analyses (e.g., A. Albert et al. 2017; A. McDaniel et al. 2024), the uncertainty on the *J*-factors estimated this way is assumed to be 0.6 dex to represent the expected measurement uncertainty after kinematic observations. For the UFCSs, this choice may be less conservative since the faintness of some of these systems will likely increase the statistical uncertainty of kinematic measurements. However, A. Albert et al. (2017) found that changing the assumed *J*-factor uncertainty had a small effect compared to the uncertainty arising from the unknown nature of the UFCSs (i.e., some may be devoid of DM). M. Crnogorčević & T. Linden (2024) compare the uncertainty on the sensitivity obtained from UMa III using different uncertainties for the *J*-factor (namely, the value of ~1.5 dex proposed by R. Errani et al. 2023b and 0.6 dex, typically used for the dSphs—see their Figure 1). This has a minor effect on the sensitivity profile and its uncertainty compared to the fact that some of the UFCSs may be devoid of DM entirely, which we discuss in more detail in Section 5. Consequently, we adopt the value for the *J*-factor uncertainty of 0.6 dex assumed in A. Albert et al. (2017) and A. McDaniel et al. (2024) to reflect our hypothesis of similarity to the dSphs, also assuming that future velocity dispersion measurements made on the UFCSs will reach a precision similar to that of the dSphs. In Figure 2, we show the assumed *J*-factors and assumed uncertainties for each target in our sample.[11]

4. Fermi-LAT Data Analysis

We analyze data from the Fermi-LAT (W. B. Atwood et al. 2009; M. Ajello et al. 2021) taken between 2008 August 4 and 2022 December 1 (14.3 yr). Our data set and analysis pipeline closely follow the dSph analysis performed by A. McDaniel et al. (2024), which makes use of the `Fermitools` (v2.2.0) via the `fermipy` (v1.2) interface (M. Wood et al. 2017). Photons from the P8R3_SOURCE_V3 class are selected with

[11] These values are based on the assumption that the UFCSs are similar in nature to the dSphs. If the subhaloes are stripped down to their stellar components, their *J*-factors could be lower by about an order of magnitude.

energies between 500 MeV and 1 TeV. Events observed at an angle from the zenith of the spacecraft greater than 100° are removed to avoid contamination from Earth's limb. Data from all four point-spread function (PSF) event classes are selected and used in a joint-likelihood analysis. This approach splits the photon events into PSF classes and includes additional information about the event-wise quality of the angular reconstruction and uses dedicated instrument response functions for each PSF event class (M. Ackermann et al. 2015).

The first step of the analysis is to define a $10^\circ \times 10^\circ$ region of interest (ROI) centered on each UFCS target. Events are divided into eight logarithmically spaced bins of energy and spatial bins of $0.^\circ08$. The ROI is modeled including the Galactic diffuse emission (`gll_iem_v07.fits`), the isotropic spectrum for the PSF type that is being considered (`iso_P8R3_SOURCE_V3_PSF{i}_v1.txt`, with i going from 0 to 3), and point-like and extended sources from the 4FGL-DR3 (`gll_psc_v29.fits`; S. Abdollahi et al. 2020, 2022). In particular, all sources that are up to 15° from the target are included to account for γ-ray emission originating outside the ROI. Each UFCS target is modeled as a point-like source with a power-law spectrum. These assumptions were made to allow for a close comparison to the dSph results from A. McDaniel et al. (2024). Previous studies on the effects of the spatial extension of targets on DM limits have been performed for the dSphs and have shown that modeling the sources as extended can lead to weaker limits in the DM parameter space (M. Di Mauro et al. 2022). However, this additional uncertainty is subdominant to the uncertainty coming from our lack of knowledge of the DM density profile of each UFCS in the sample. The model is optimized, keeping as free parameters the photon index and normalization of the Galactic diffuse emission and the normalization of the isotropic component, as well as the normalization of all sources with test statistics[12] TS $\geqslant$25 that are up to 5° away from the target, and the normalization and photon index of all sources with TS $\geqslant$ 500 that are up to 7° away from the target. The `find_sources()` method is used to look for additional sources in the ROI, and if any is found with TS $>$ 16, it is included in the model. The new sources closest to a target, both with TS ~ 20, are found with an offset of $0.^\circ51$ and $0.^\circ22$ from DELVE 2 and DELVE 3, respectively.[13] Neither source overlaps with the target within their 95% localization contour (~$0.^\circ1$). All the other new sources are found at an offset $> 1^\circ$. The next step in the analysis is to calculate the spectral energy distribution for each target through the use of the `fermipy sed()` function (for more information on this method, see M. Ackermann et al. 2014). Fits are performed independently in each energy bin, with the target modeled by a power-law spectrum with a fixed index of 2 and free normalization, while leaving the diffuse background normalizations free to vary. This procedure yields a likelihood profile, $\mathcal{L}(d\Phi_\gamma/dE, E)$, in flux–energy space. The likelihood for a given DM mass and cross section can be then computed by replacing $d\Phi_\gamma/dE$ with the theoretical γ-ray yield from DM annihilation (Equation (1))—which is a function of DM mass, cross section, and energy—then summing over energy bins. This can be summarized by the following expression:

$$\mathcal{L}(\langle\sigma v\rangle, M_\chi) = \sum_{E_i} \mathcal{L}\left[\frac{d\Phi_\chi}{dE}(\langle\sigma v\rangle, M_\chi, E_i), E_i\right]. \quad (4)$$

This likelihood profile is used to define a TS profile for the target,

$$\mathrm{TS}(\langle\sigma v\rangle, M_\chi) = 2\left[\frac{\mathcal{L}(\langle\sigma v\rangle, M_\chi)}{\mathcal{L}_0}\right], \quad (5)$$

where $\mathcal{L}_0$ is the likelihood for the null hypothesis (i.e., no γ-ray source). The parameter space considered covers a mass range of $M_\chi \in [5;\ 10^4]$ GeV and a cross-section range of $\langle\sigma v\rangle \in [10^{-28};\ 10^{-22}]$ cm^3 s^{-1}, which is motivated by the GeV–TeV-scale thermal relic WIMP DM models and the constraining capability of Fermi-LAT observations. To incorporate uncertainties in the J-factors, the Fermi-LAT likelihood function is multiplied by a J-factor likelihood function, $\mathcal{L}_J$:

$$\mathcal{L}_J(J) = \frac{1}{\ln(10)\sqrt{2\pi\sigma_J}J_{\rm obs}} \times \exp\left[-\left(\frac{\log_{10}(J) - \log_{10}(J_{\rm obs})}{\sqrt{2}\,\sigma_J}\right)^2\right]. \quad (6)$$

The J-factor likelihood function is defined as a Gaussian in the $\log J$ space, where $J_{\rm obs}$ is the J-factor value estimated from the scaling relations in A. B. Pace & L. E. Strigari (2019) and σ_J is the uncertainty on the J-factor, assumed to be 0.6 dex in this analysis.

The limits obtained from the γ-ray data coincident with UFCSs can be compared to statistical expectations of the background using a "blank-field" analysis (e.g., M. Ackermann et al. 2014). The analysis of blank fields accounts for the effects of undetected sources in the Fermi-LAT data and for the uncertainty in the models of the diffuse background emission by sampling of regions of the sky that contain no known γ-ray sources or likely γ-ray emitters based on spatial coincidence with the Fermi-LAT and multiwavelength catalogs. The blank fields are randomly selected at high Galactic latitude ($|b| > 15\circ$) by applying similar criteria to those used to select the sample of UFCSs—i.e., excluding regions centered within the 95% confidence radius of a 4FGL-DR3 source or within $0.^\circ1$ from any source in the BZCat, CRATES, and WIBRaLS catalogs. We use the same 1000 regions selected for the dSph analysis in A. McDaniel et al. (2024).[14] From these regions, sets of 26 blank fields (i.e., the same size as the UFCS sample) are randomly selected without replacement 10^4 times to perform a combined blank-field analysis. We refer to A. McDaniel et al. (2024) for more details on the blank-field analysis.

5. Results and Discussion

We analyzed ~15 yr of γ-ray from Fermi-LAT data coincident with a selection of UFCSs that are potentially DM dominated. If their nature is confirmed, the UFCSs are expected

[12] The TS of the sources is defined as $\mathrm{TS} = 2\log(\mathcal{L}/\mathcal{L}_0)$, where $\mathcal{L}$ is the likelihood derived including the target of interest in the model fit, and $\mathcal{L}_0$ is the likelihood of the null hypothesis (i.e., fixing the flux of the target source at zero).

[13] Including or removing DELVE 3 from the analysis has negligible effects on the combined constraints.

[14] The data are taken from the public figshare page: https://figshare.com/articles/dataset/Legacy_Analysis_of_Dark_Matter_Annihilation_from_the_Milky_Way_Dwarf_Spheroidal_Galaxies_with_14_Years_of_Fermi-LAT_Data_Data_Products/24058650/1.

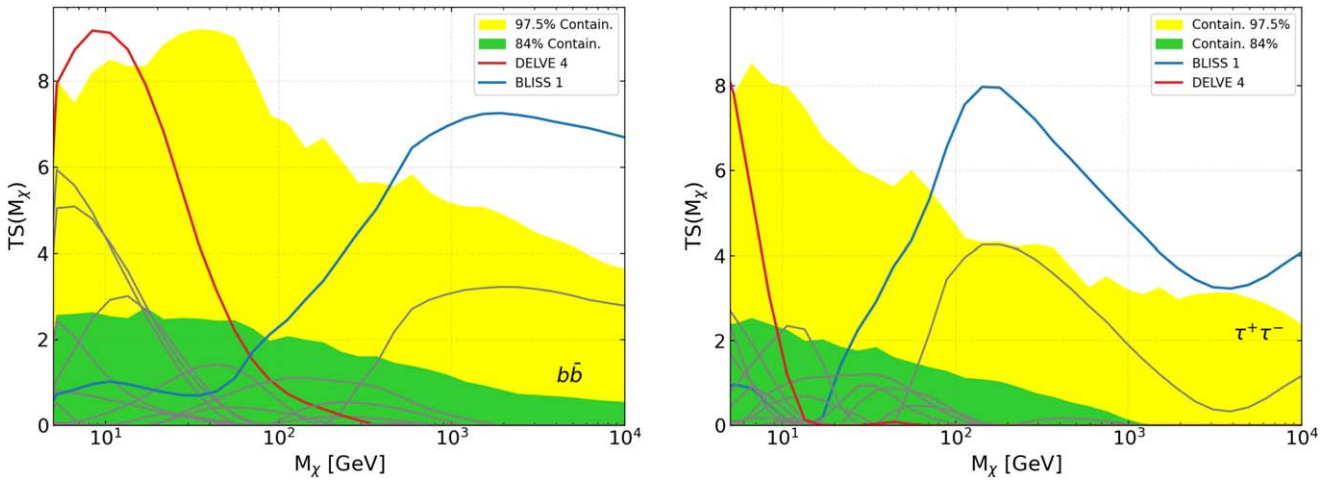

Figure 3. Maximum TS over all cross-section values versus mass for the individual UFCSs in the $b\bar{b}$ (left) and $\tau^+\tau^-$ (right) channels. The colored lines highlight the targets that show a TS excess over the 97.5% and 84% containment regions for the individual blank fields (green and yellow bands).

to put stringent constraints on DM properties since their relative proximity could lead to a higher flux of γ-rays from DM annihilation compared to the previously studied dSphs. However, no significant γ-ray emission is observed in the combined sample of UFCSs. We present the upper limits for the γ-ray flux from each source in Figure 2, with the respective values reported in Table 1.

To assess the significance of a signal from the individual targets in our sample, we evaluate the maximum TS over all cross-section values as a function of the mass and compare it to the 84% and 97.5% containment bands from the 1000 individual blank fields (see Figure 3). Only DELVE 4 and BLISS 1 (colored lines in Figure 3) show local significance $\gtrsim 2\sigma$ over the background though we notice that these peaks in significance occur in different ranges of M_χ, which would not be expected if they could both be attributed purely to DM annihilation.

We derive the sensitivity to the null detection of γ-ray emission in UFCSs to put constraints on DM properties in the velocity-averaged cross section vs. mass space, for the $b\bar{b}$ and $\tau^+\tau^-$ annihilation channels. In Figure 4, we compare the upper limits obtained from the UFCSs in the inclusive and nominal samples for both channels to the results for dSphs (A. McDaniel et al. 2024), for the Galactic center excess (GCE; F. Calore et al. 2015; M. Di Mauro 2021), and to the cross section for thermal relic DM (G. Steigman et al. 2012). The sensitivities obtained from the two selections are similar, with the nominal sample yielding a slightly less stringent constraint. We also present the results obtained excluding UMa III from the nominal sample since this source dominates the sample due to its proximity and high J-factor. M. Crnogorčević & T. Linden (2024) have demonstrated that, according to the current estimation of its J-factor, UMa III alone can put constraints on DM properties that are competitive with the most recent results from dSphs. In this context, evaluating the effects of excluding this target from the sample is crucial for two reasons. First, it gives an upper limit on how the results presented here would be affected if further investigation of UMa III leads to a lower estimation of its J-factor. Second, it evaluates the contribution to the constraints from the remaining targets of the nominal sample, showing that they provide a pronounced improvement to the constraints relative to the dSphs. The upper limits obtained from both the inclusive and nominal samples are better than the constraints obtained from previous analyses at all masses and in both channels. Even with the exclusion of UMa III, the limits obtained from the nominal sample are lower than the dSph constraints for the majority of the mass range.

We also take into account the effects of the background through the combined blank-field analysis, from which we derive the 68% and 95% containment bands in the top panels of Figure 4. The UFCSs limits are mostly contained within these bands, and the only slight excess is observed at the highest masses in the $b\bar{b}$ channel when UMa III is excluded from the analysis (Figure 4).

As said, our analysis is premised on the assumption that the UFCSs are DM dominated and behave similarly to the dSphs. Yet, given the lack of direct spectroscopic measurements, the DM content of these systems cannot be confirmed at present, and it is possible that some of these systems are DM-deficient star clusters or that they are "microgalaxies."

To account for the possibility that not all of the systems are hosted in DM subhaloes or that some of the subhaloes are not as resilient to stripping as the dSphs, we also compute the sensitivity for random subsets of the UFCSs in the inclusive sample, effectively treating the excluded systems as devoid of DM. This allows us to gauge the main source of uncertainty in the results, which comes from the undetermined nature of the targets in our sample.

In the central panels of Figure 4, we compute the constraints for 1000 subsets of 13 UFCSs selected randomly from the 26 UFCSs in the inclusive sample. This allows us to evaluate the variability of the results due to the exclusion of some of the sources. We highlight the selections that contain UMa III as these tend to lead, on average, to better constraints compared to the selections that do not contain this system. Again, we compare these bands to results for the dSphs and the GCE, as well as the thermal relic cross section. In the $b\bar{b}$ channel, the selections that do not include UMa III are similar to the results from the dSphs, with their average being more constraining up to high values of the DM mass ($M_\chi \gtrsim 1$ TeV). In the $\tau^+\tau^-$ channel, this inversion happens at about an order of magnitude lower mass ($M_\chi \sim 100$ GeV). Yet, once again, the constraints are compatible when considering the variability coming from the different selections. In both channels, most of the DM limits from selections that include UMa III are still better than the

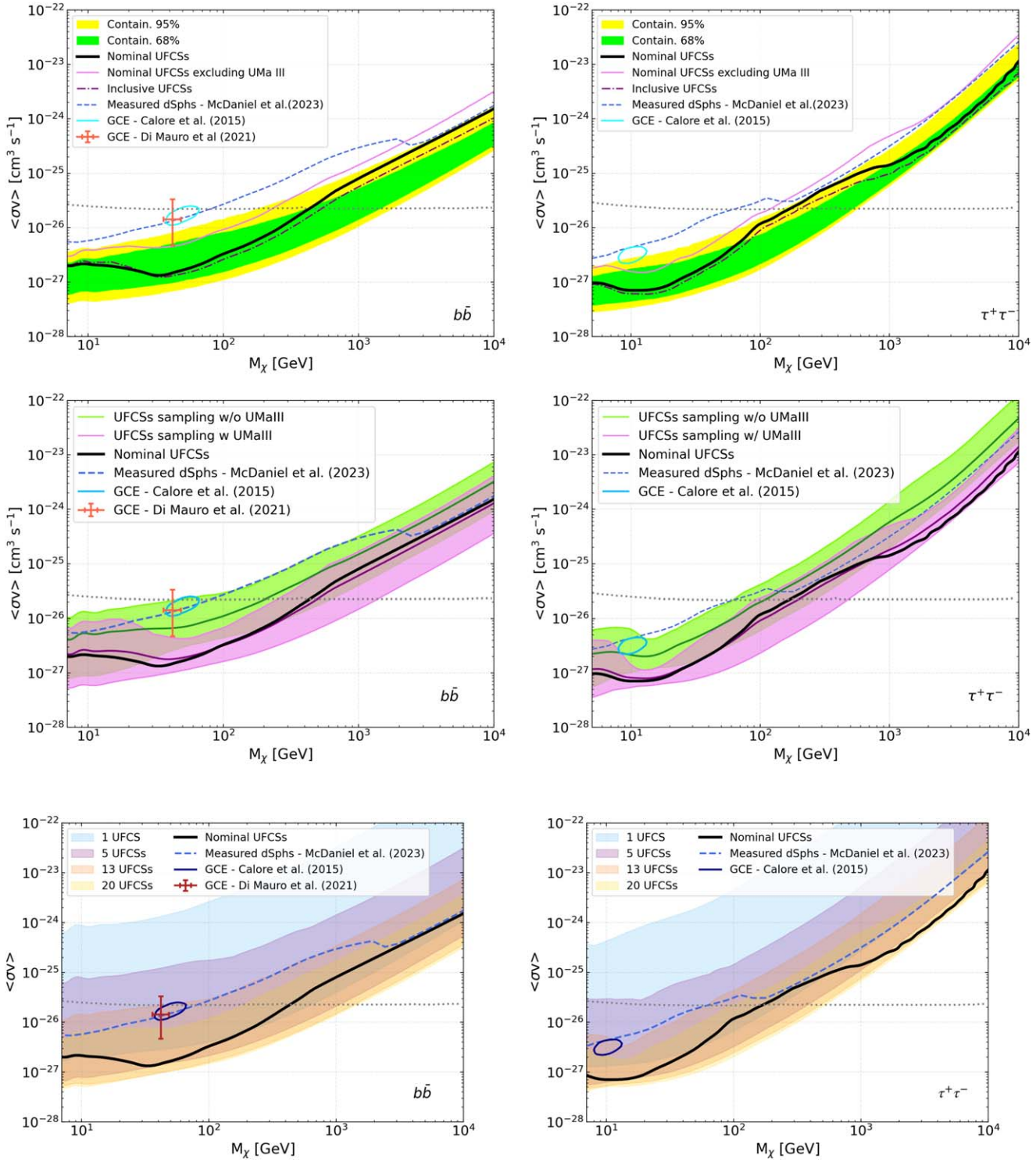

Figure 4. Top: sensitivity of Fermi-LAT observations of UFCSs to DM annihilation via the $b\bar{b}$ (left) and $\tau^+\tau^-$ (right) channels. The solid black lines represent the constraints obtained from the combined analysis of the UFCSs in the nominal sample. The pink lines are constraints obtained excluding UMa III from this selection. The dotted–dashed purple lines are the constraints obtained from the combined analysis of UFCSs in the inclusive sample. The yellow and green regions are, respectively, the 95% and 68% containment bands for the inclusive sample obtained from the combined analysis of random subsets of 26 of the 1000 blank fields. The dotted line is the thermal relic cross section from G. Steigman et al. (2012). The dashed blue lines are constraints from A. McDaniel et al. (2024) for the measured sample of dSphs. The light blue profile represents the DM interpretation of the GCE from F. Calore et al. (2015), while the red point with error bars is the GCE measurement from M. Di Mauro & M. W. Winkler (2021). Center: sensitivity of Fermi-LAT observations to DM annihilation via the $b\bar{b}$ (left) and $\tau^+\tau^-$ (right) channels derived by randomly selecting half of the UFCSs in the inclusive sample. The green band represents the selections that do not include UMa III, while the pink band represents the selections that include this source. The solid lines represent the average constraint from the respective band of the same color. The solid black line represents the constraints from the nominal sample of UFCSs. We also include results from previous analyses on the dSphs (A. McDaniel et al. 2024) and GCE (F. Calore et al. 2015; M. Di Mauro & M. W. Winkler 2021). Bottom: sensitivity of Fermi-LAT observations to DM annihilation via the $b\bar{b}$ (left) and $\tau^+\tau^-$ (right) channels derived for different sizes of the random subsamples.

dSph constraints, and their average is comparable to the limits obtained from the nominal sample. A similar comparison can be made with observations of the GCE, which lie close to the average constraint of the selections that include UMa III. The extension of the uncertainty bands is related to the size of the selections, as shown in the bottom panels of Figure 4. Here, we display the same evaluation described above for varying subsample sizes.[15]

This study highlights the need for further investigations of the nature of UFCSs, since confirming that even a few of the observed systems are hosted in DM haloes that have not undergone significant tidal stripping could significantly increase the sensitivity of studies on DM annihilation. Furthermore, optical imaging surveys such as DELVE (A. Drlica-Wagner et al. 2021), UNIONS (R. A. Ibata et al. 2017), and Rubin LSST (S. M. Kahn & J. A. Tyson 2019) are likely to discover more UFCSs (e.g., J. R. Hargis et al. 2014; E. O. Nadler et al. 2020; V. Manwadkar & A. V. Kravtsov 2022). Ongoing spectroscopic observing campaigns with the Keck and Magellan telescopes, as well as with the Dark Energy Spectroscopic Instrument (DESI Collaboration et al. 2016), should be able to provide initial kinematic measurements following procedures similar to those described in J. D. Simon (2019); however, comprehensive measurements of the DM content of very faint systems will likely require 30 m class telescopes (e.g., A. Drlica-Wagner et al. 2018).

Acknowledgments

A.C., A.M., C.K., and M.A. acknowledge support from NASA grant 80NSSC22K1580 (Fermi Guest Investigator Program Cycle 15 No. 151048). Clemson University is acknowledged for generous allotment of compute time on Palmetto cluster. A.D.W. acknowledges support from NASA contract NNG17PZ02I (Fermi Guest Investigator Program Cycle 9 No. 91201) and NSF grant No. AST-2307126. M.D.M. acknowledges support from the Research grant TAsP (Theoretical Astroparticle Physics) funded by Istituto Nazionale di Fisica Nucleare (INFN). MASC was supported by the grants PID2021-125331NB-I00 and CEX2020-001007-S, funded by MCIN/AEI/10.13039/501100011033, by "ERDF A way of making Europe," and the MULTIDARK Project RED2022-134411-T.

The Fermi-LAT Collaboration acknowledges generous ongoing support from a number of agencies and institutes that have supported both the development and the operation of the LAT as well as scientific data analysis. These include the National Aeronautics and Space Administration and the Department of Energy in the United States, the Commissariat à l'Energie Atomique and the Centre National de la Recherche Scientifique / Institut National de Physique Nucléaire et de Physique des Particules in France, the Agenzia Spaziale Italiana and the Istituto Nazionale di Fisica Nucleare in Italy, the Ministry of Education, Culture, Sports, Science and Technology (MEXT), High Energy Accelerator Research Organization (KEK) and Japan Aerospace Exploration Agency (JAXA) in Japan, and the K. A. Wallenberg Foundation, the Swedish Research Council and the Swedish National Space Board in Sweden.

Additional support for science analysis during the operations phase is gratefully acknowledged from the Istituto Nazionale di Astrofisica in Italy and the Centre National d'Études Spatiales in France. This work performed in part under DOE Contract DE-AC02-76SF00515.

Software: `numpy`, `scipy`, `astropy`, `Fermitools`, `fermiPy` (M. Wood et al. 2017), `dmsky`,[16] `local_volume_database`.[17]

ORCID iDs

Alex Drlica-Wagner https://orcid.org/0000-0001-8251-933X
Christopher Karwin https://orcid.org/0000-0002-6774-3111
Marco Ajello https://orcid.org/0000-0002-6584-1703
Mattia Di Mauro https://orcid.org/0000-0003-2759-5625
Miguel Á. Sánchez-Conde https://orcid.org/0000-0002-3849-9164

References

Abdo, A. A., Ackermann, M., Ajello, M., et al. 2010, ApJ, 712, 147
Abdollahi, S., Acero, F., Ackermann, M., et al. 2020, ApJS, 247, 33
Abdollahi, S., Acero, F., Baldini, L., et al. 2022, ApJS, 260, 53
Ackermann, M., Albert, A., Anderson, B., et al. 2014, PhRvD, 89, 042001
Ackermann, M., Albert, A., Anderson, B., et al. 2015, PhRvL, 115, 231301
Ajello, M., Atwood, W. B., Axelsson, M., et al. 2021, ApJS, 256, 12
Albert, A., Anderson, B., Bechtol, K., et al. 2017, ApJ, 834, 110
Arina, C., Di Mauro, M., Fornengo, N., et al. 2024, JCAP, 2024, 035
Atwood, W. B., Abdo, A. A., Ackermann, M., et al. 2009, ApJ, 697, 1071
Balbinot, E., Santiago, B. X., da Costa, L., et al. 2013, ApJ, 767, 101
Ballet, J., Bruel, P., Burnett, T. H., Lott, B. & The Fermi-LAT collaboration 2023, arXiv:2307.12546
Bergström, L. 2000, RPPh, 63, 793
Bergström, L., Ullio, P., & Buckley, J. H. 1998, APh, 9, 137
Bertone, G., Hooper, D., & Silk, J. 2005, PhR, 405, 279
Bonnivard, V., Combet, C., Daniel, M., et al. 2015, MNRAS, 453, 849
Calore, F., Cholis, I., McCabe, C., & Weniger, C. 2015, PhRvD, 91, 063003
Cerny, W., Drlica-Wagner, A., Li, T. S., et al. 2023a, ApJL, 953, L21
Cerny, W., Martìnez-Vázquez, C. E., Drlica-Wagner, A., et al. 2023b, ApJ, 953, 1
Ciafaloni, P., Comelli, D., Riotto, A., et al. 2011, JCAP, 2011, 019
Cirelli, M., Corcella, G., Hektor, A., et al. 2011, JCAP, 2011, 051
Conn, B. C., Jerjen, H., Kim, D., & Schirmer, M. 2018, ApJ, 852, 68
Crnogorčević, M., & Linden, T. 2024, PhRvD, 109, 083018
DESI Collaboration, Aghamousa, A., Aguilar, J., et al. 2016, arXiv:1611.00036
Di Mauro, M. 2021, PhRvD, 103, 063029
Di Mauro, M., Pérez-Romero, J., Sánchez-Conde, M. A., & Fornengo, N. 2023, PhRvD, 107, 083030
Di Mauro, M., Stref, M., & Calore, F. 2022, PhRvD, 106, 123032
Di Mauro, M., & Winkler, M. W. 2021, PhRvD, 103, 123005
Drlica-Wagner, A., Albert, A., Bechtol, K., et al. 2015, ApJL, 809, L4
Drlica-Wagner, A., Bechtol, K., Mau, S., et al. 2020, ApJ, 893, 47
Drlica-Wagner, A., Carlin, J. L., Nidever, D. L., et al. 2021, ApJS, 256, 2
Drlica-Wagner, A., Freedman, W., Gladders, M., Li, T., & Scolnic, D. 2018, in Giant Magellan Telescope Science Book, ed. R. Bernstein et al. (Las Campanas: GMTO), 149, https://www.staging.giantmagellan.org/wp-content/uploads/2021/11/GMTScienceBook2018.pdf
Errani, R., Ibata, R., Navarro, J. F., Peñarrubia, J., & Walker, M. G. 2023a, ApJ, 968, 89
Errani, R., Navarro, J. F., Smith, S. E. T., & McConnachie, A. W. 2023b, ApJ, 965, 20
Evans, N. W., Sanders, J. L., & Geringer-Sameth, A. 2016, PhRvD, 93, 103512
Hargis, J. R., Willman, B., & Peter, A. H. G. 2014, ApJL, 795, L13
Harris, W. E. 1996, AJ, 112, 1487
Homma, D., Chiba, M., Komiyama, Y., et al. 2019, PASJ, 71, 94
Ibata, R. A., McConnachie, A., Cuillandre, J.-C., et al. 2017, ApJ, 848, 128
Ivezić, Ž., Kahn, S. M., Tyson, J. A., et al. 2019, ApJ, 873, 111

[15] This evaluation is assuming that some of the UFCSs behave like dSphs, and the rest are DM devoid. The uncertainties would be larger than those assumed here if the UFCSs are not hosted by large DM subhaloes à la dSphs.

[16] https://github.com/fermiPy/dmsky

[17] https://github.com/apace7/local_volume_database

Jungman, G., Kamionkowski, M., & Griest, K. 1996, PhR, 267, 195
Kim, D., & Jerjen, H. 2015, ApJ, 799, 73
Kim, D., Jerjen, H., Mackey, D., Costa, G. S. D., & Milone, A. P. 2016, ApJ, 820, 119
Kim, D., Jerjen, H., Milone, A. P., Mackey, D., & Da Costa, G. S. 2015, ApJ, 803, 63
Kravtsov, A., & Manwadkar, V. 2022, MNRAS, 514, 2667
Laevens, B. P. M., Martin, N. F., Sesar, B., et al. 2014, ApJL, 786, L3
Longeard, N., Martin, N., Ibata, R. A., et al. 2019, MNRAS, 490, 1498
Luque, E., Pieres, A., Santiago, B., et al. 2017, MNRAS, 468, 97
Luque, E., Santiago, B., Pieres, A., et al. 2018, MNRAS, 478, 2006
Manwadkar, V., & Kravtsov, A. V. 2022, MNRAS, 516, 3944
Martin, N. F., Jungbluth, V., Nidever, D. L., et al. 2016, ApJL, 830, L10
Mau, S., Drlica-Wagner, A., Bechtol, K., et al. 2019, ApJ, 875, 154
Mau, S., Cerny, W., Pace, A. B., et al. 2020, ApJ, 890, 136
McDaniel, A., Ajello, M., Karwin, C. M., et al. 2024, PhRvD, 109, 063024
Muñoz, R. R., Côté, P., Santana, F. A., et al. 2018, ApJ, 860, 66
Nadler, E. O., Wechsler, R. H., Bechtol, K., et al. 2020, ApJ, 893, 48
Pace, A. B. 2024, arXiv:2411.07424
Pace, A. B., & Strigari, L. E. 2019, MNRAS, 482, 3480
Revaz, Y. 2023, A&A, 679, A2
Sawala, T., Frenk, C. S., Fattahi, A., et al. 2015, MNRAS, 456, 85
Simon, J. D. 2019, ARA&A, 57, 375
Smith, S. E. T., Cerny, W., Hayes, C. R., et al. 2024, ApJ, 961, 92
Steigman, G., Dasgupta, B., & Beacom, J. F. 2012, PhRvD, 86, 023506
Torrealba, G., Belokurov, V., & Koposov, S. E. 2019, MNRAS, 484, 2181
Willman, B., Blanton, M. R., West, A. A., et al. 2005, AJ, 129, 2692
Wood, M., Caputo, R., Charles, E., et al. 2017, ICRC (Busan), 301, 824